Crashworthiness Analysis of Foam–Filled Prismatic Structures

Tatacipta Dirgantara[1], Annisa Jusuf, Leonardo Gunawan, Ichsan Setya Putra

Lightweight Sructures Research Group, Faculty of Mechanical and Aerospace Engineering

Institut Teknologi Bandung, Ganesha 10, Bandung 40132, Indonesia

[1]Corresponding author

  Email: tdirgantara@ftmd.itb.ac.id

  Phone: +62–22–2512971, Fax: +62–22–2512972

Abstract

This paper presents results on the crushing behavior of aluminum foam–filled columns with square cross section. Here, the effect of inserting an aluminum foam to a single–walled and double–walled columns were studied. Parametric study for both types of columns compared with single–walled and double–walled columns were also carried out. The numerical results were compared with available experimental data. Further investigation has been conducted on the effect of core thickness to the mean crushing force response of the columns. The results showed that the interaction between the foam core and the column wall will change the deformation mode from one localized fold to multiple propagating folds and lead to the increase of total mean crushing force of the column. Similar effect of foam filling was also found in double–walled foam–filled columns. It is also found that by increasing the core thickness, the crushing force will be higher.

Keywords: Thin–walled column; Single–walled; Double–walled; Foam–filled; Impact; Dynamic axial crushing

1. Introduction

Thin–walled column has been known as a promising and efficient impact energy absorbing structure in space frame concept of a car, train structures and helicopter subfloor [1] – [6]. There are two main important issues that shall be addressed in the design of a prismatic column for an energy absorption device, i.e.: how to achieve the required mean crushing force, and how to

reduce the high first peak force. The first one related to the crushing resistance capacity of the column, while the second one related to the decceleration level experienced by the passenger.

In general, the simplest way to increase the axial crushing resistance is by thickening the column wall, however this is not the best way since the mass of the column will also increase. To reduce the high first peak force, usually a trigger is introduced to the thin–walled structures. With the availability of new material, as an alternative, a modification of the column's cross section by inserting a low density filler can be done to increase the axial crushing resistance while maintaining the weight efficiency and eliminating the high first peak force. This alternative way of filling polyurethane foam to reinforce thin–walled components was first recommended by Thornton [7].

By using foam filler, it is expected that the rigidity of the thin–walled member can be increased while minimizing additional weight. When a thin–walled member is filled completely with a foam core, an interaction between the filler and the column walls is also expected, which will produce some worthwhile crushing characteristics and energy absorption properties because of inward and outward fold formations are constrained during axial crushing process.

In recent decades, metal foam such as aluminum foam has been developed as a new ultra–lightweight engineering material. This material has unique mechanical properties, i.e. it can undergo large strain deformation while maintaining its low constant stress before the densification. One main application of this material is as an energy absorber structure. Filling the columns with aluminum foam will improve energy absorption characteristics and stabilizes the buckling process of the column. A superior weight efficiency was obtained for thin–walled members filled with the metal foam core, as studied numerically by Santosa et al. [8] − [10]. In his study, behavior of filled columns undergoing axial compression was analyzed. The mean

3

crushing loads of the filled columns are found to be higher than the sum of the crushing loads of foam and column alone, as confirmed by Chen [11] and Kavi et al. [12].

Recently, Niknejad et al. [11] developed a theoretical formula to predict the instantaneous crushing force of a polyurethane foam–filled square column and polyurethane foam–filled grooved circular columns under axial loading. The calculated theoretical relation was then compared with the experimental results, and showed a good correlation.

In maximizing the potential implementation of the foam core as lightweight fillers, an alternative concept of double–walled foam–filled column, in which a foam filler is inserted between the inner wall and the outer wall of the column, has been proposed to increase weight efficiency of crashworthy structures by Santosa and Wierzbicki [15], but so far there is not much information available on the behavior of double–walled sections under crushing force in general and especially dynamic crushing load. Most of the research focused on axial crushing performance of foam–filled section of square column and circular column, both experimentally and numerically. The behavior of double–walled foam–filled column itself has only been reported by Santosa and Wierzbicki [15] using a non–linear dynamic finite element analysis. In [15], the mean crushing force of a square double–walled column with metal foam filler was found to increase significantly, compared to the corresponding thin–walled column with the same mass.

Later, a quasi–static experimental investigations on double–walled foam–filled columns with different materials, dimensions and cross–sectional shapes were carried out by Seitzberger et al. [16]. The test results confirmed that double–walled foam–filled column, are shown to be an efficient energy absorbing device, as long as global failure can be avoided.

More recently, the optimization of the crashworthiness of the double–walled, single–walled foam–filled and double–walled foam–filled square columns were conducted by Zhang et al. [17]. The results demonstrate that the double–walled foam–filled configuration has more room to enhance the crashworthiness and can become an efficient energy absorber.

To understand the behavior of single–walled and double–walled foam–filled columns under low velocity impact load, in this work a parametric study of such structures has been conducted. Firstly, the numerical simulations of the columns were conducted and validated by the experiments that has been previously reported by Gunawan et al. [18]. The crushing response in the experiment validate that the finite element simulation of the columns under axial dynamic loading has sufficient accuracy. Hence, the finite element simulations could then be employed further to perform parametric analyses of the columns. Secondly, the effect of the core thickness to the behavior of the structures under crushing load in general and especially dynamic crushing load will be investigated numerically. Then, the effect of foam core thickness variations to the crushing resistance was also studied. Hence, it is expected that the crushing characteristics of single–walled and double–walled columns filled with foam core can be understood better.

2. Geometrical Detail

In this paper, four cross section configurations were studied, i.e. single–walled (SW) column, double–walled (DW) column, single–walled foam–filled (SWFF) column, and double–walled foam–filled (DWFF) column. The experimental results of SW, DW, SWFF and DWFF column have been reported previously by Gunawan et al. [18]. Geometry of the columns is shown in Fig 1. The length of all columns is 180 mm.

The column wall was made of extruded aluminum alloy AA 6063 T1. In the case when the columns are filled with a foam filler material, the foam core was inserted to the empty column without adhesive bonding between the wall of the column and the foam core. In this paper, the investigation was divided into three groups of analysis.

The first set of analysis is the numerical simulations of AA 6063 T1 columns. The parameters were set to be exactly the same as those in the experiments [18], in order to validate the numerical results with ones obtained from the experiment. The details of column geometry of square single–walled column and double–walled column are presented in Table 1 and Table 2 (Set 1).

In the second set of analysis, numerical simulations were conducted to investigate the effect of inserting aluminum foam to a single–walled column and double–walled column to the crushing response of the columns. The column thickness, column width, impact velocity and impacting mass are set to be constant for all columns. The details of column geometry and associated parameter are shown in Table 2 (Set 2).

The focus of Set 3 is to explore the effect of different core thickness (C) in double–walled foam–filled column, which are $C = 7$ mm, 8.5 mm, 10 mm, to the mean crushing force and energy absorbing capacity compared to single–walled foam–filled column. The details of column geometry are shown in Table 2 (Set 3).

The dimensions of sides a, b, c, d of the column in Set 1 are not exactly the same, because they are obtained from the actual measurement of the specimen which were used in the experiment, as shown in Fig. 1, Table 1 and Table 2.

3. Mechanical Properties

In this paper, extruded aluminum alloy square columns (AA 6063 T1) filled with a closed –
cell aluminum foam (ALPORAS) block were used. The type of ALPORAS used in the research
is classified as high density foam with density of ~440 kg/m^3 and relative density 0.16. The foam
has average cell size of ~2.43 mm.

The mechanical properties of ALPORAS was previously determined by a displacement
controlled compression tests that were performed to 50 mm × 25 mm × 25 mm specimens with
displacement rate 0.08 mm/s and strain rate 1.6 /s. During the tests, the specimens were
unloaded, and then reloaded several times, and then were continued up to the final strain. A
typical stress – strain curve obtained from uniaxial compression test is shown in Fig. 2. The
material properties of ALPORAS can be seen in Table 3.

In this work, the material used for the column wall is 6063 T1 aluminum alloy extrusion. Two
tensile test types were carried out in order to obtain accurate material information and also define
the input for material modeling in the numerical simulations, i.e. quasi static (0.001 /s) and
dynamic (0.1, 1, 10, 100 /s) tensile tests. It was found that the engineering stress – strain curve of
Aluminium alloys was insensitive to the strain rate and hence it does not need to include strain
rate effects into the material model. The detail of mechanical properties of the material is
presented in Table 3 and the true stress–true plastic strain curve is shown in Fig. 3.

4. Finite Element Modeling

To be able to properly simulate foam–filled columns, a commercial finite element code LS–
DYNA was used, which can perform explicit non–linear dynamic analysis. The typical finite
element model of foam–filled columns are shown in Fig. 4. In this study, the fixed constraints

were located at the bottom of all columns, while the other end was crushed in the axial direction by a rigid wall with an initial velocity as shown in Table 2.

The column walls are modeled by using Belytschko–Lin–Tsay–4–node thin shell elements and a piecewise linear plasticity model was utilized to describe the material behavior. The element size of 2×2 mm^2 are found to be sufficient and suitable for the plastic deformation modes simulation of the columns.

Hanssen et al. [18], have studied comprehensively different foam models available in the explicit finite element software package, and concluded that none of the models could characterize all load configurations with convincing accuracy. Even for quite simple loading conditions, the plastic deformation configuration differed from each other. In this work, the crushable foam material was selected for numerical simulation, since several previous researches [19, 20] have shown that among several foam material models, this model was found to perform pretty well with good computational efficiency.

Four different type of contact algorithms were used in the model. The first was automatic nodes to surface contact to model the interactions between the rigid impactor and the column. Here, for every time step, every node on the column was checked to ensure that there was no penetration to the surface of the impactor.

To understand the appropriate coefficient of frictions between the column and the rigid body, studies on crushing response and deformation modes of single–walled aluminum columns were carried out. The results can be seen in Fig. 5(a) for instantaneous crushing force and the Fig. 5(b) for deformation modes. It was found that the mean crushing forces, as shown in Table 4, was not affected by the value of friction coefficients. However the friction constants affect deformation mode. When the frictionless contact was employed, an unrealistic first deformation mode was

8

observed at the upper end of the column, as can be seen in Fig. 5(b). By introducing static and dynamic friction constants, the crushing force is not significantly affected, and the deformation mode become realistic and similar to that of the experiments. Simulations using different sets of static and dynamic friction constants, i.e. 0.61 and 0.47 [19] − [21], 0.25 and 0.25 [23]; 1.0 and 1.0 produce similar results. Hence, in this work, the static and dynamic coefficient of friction of mild steel to aluminum of 0.61 and 0.47 were respectively chosen.

The second contact algorithm is the automatic single surface contact to handle self–contact of the column wall due to folding deformation. The third contact algorithm is automatic surface to surface contact to simulate the contact between the column wall and the aluminum foam. Finally, an interior contact is adopted to the model to prevent the occurence of volumetric error in foam–filled solid model.

An introduction of inextensional geometrical imperfection to the finite element models of the columns were made, in order to simulate foam–filled columns appropriately. The imperfection type was decided after observing the mode of deformation from the experimental results which showed that the first deformation mode was an inextensional mode. The imperfection was located at the folding length, $2H$, above the clamped position. The length of the half sine wave ($2H$) where geometrical imperfection located was determined from the theoretical calculation of the half folding length for the symmetric mode, H, as given in [24]

$$H = 0.99b^{2/3}t^{1/3} \tag{1}$$

It was found that the value of H estimated from the theoretical prediction agreed very well with the wave length measured in the experiments.

Because the specimens for experiment were made of extruded square hollow aluminum alloy, careful modelling of the corner should be considered, since the wall thickness at corners are

9

larger than other area. It is well known that a major part of the energy absorption for square tubes takes place in the corner section. Thus a small increase in cross–sectional area might lead to a significant increase of the mean force since the additional cross–sectional area is located in the corner elements.

As shown in Fig. 6, Fig. 7 and Table 5, in the case of the extruded aluminum alloy square column model without additional thickness at the corners, the instantaneous crushing force and mean crushing force are lower compared to the experimental one.

Hence, to take into account the additional wall thickness at the corner, in the numerical model, the thickness of shell elements (t_c) adjacent to the corner were set to be equal to $\sqrt{2} \cong 1.4$ of the other wall thickness (t). The additional thickness was applied to two elements from the corner, as illustrated in Fig. 8. A very good agreement was found, in which the mean crushing force difference between numerical simulation and experiment is 1.74 %.

5. Experimental Test Set–Up

To understand the impact response of the column and to validate the numerical simulations, several impact tests were carried out. The tests were conducted using a dropped weight impact testing machine, which was designed to perform low speed impact test (< 10 m/s) [25]. Fig. 9 shows the schematic drawing and the picture of the dropped weight impact testing machine.

In the experiment, the crash box specimen was tightly fixed to the testing apparatus and placed on the vertical axis of the impactor in the impact testing machine such that the axial direction of the test specimen was parallel to the vertical direction of the impactor. The impactor impacted the crash box from the top. The maximum velocity of the impactor was 9.8 m/s. The instantaneous crushing force – time history of the specimen was recorded through load cell and

10

data acquisition system which was specifically designed and built for this machine. The maximum capacity of the load cell is 60 kN.

To measure the speed of the impactor before hitting the specimen, an velocity sensor was placed just above the specimen to record the elapsed time of the impactor assembly passing through two infrared diode sensors. The speed of the impactor was determined by dividing the distance between the two sensors with the elapsed time.

To obtain the instantaneous crushing force, strain gages in the load cell are connected to a Wheatstone bridge circuit. The output signal from the Wheatstone bridge was then amplified, filtered and stored into a PC by using a data acquisition card NI USB−6211. The data acquisition can record the data with maximum sampling rate of 250 kHz. All tests were performed at room temperature. The displacement − time history was obtained using a 1200 frames per second NIKON 1 J1 camera. The detail of the experiment is explained in [18].

6. Numerical and Experimental Analyses

In this paper, numerical simulations of SW1, DW1, SWFF1 and DWFF1 columns were conducted, and the results were validated by the experiments that have been reported previously by Gunawan et al. [18].

Plastic Deformation Modes

Fig. 10 − Fig. 13 show experimental and numerical plastic folding deformation for SW1, DW1, SWFF1 and DWFF1 columns. As can be seen, excellent agreements were found in the overall shape of the deformed columns, where the progressive plastic fold formations were observed.

11

Instantaneous and Mean Crushing Force

The instantaneous crushing force – crushing length and mean crushing force – crushing length curves of SW1, DW1, SWFF1 and DWFF1 columns can be found in Fig. 14 to Fig. 17.

Table 6 presents the mean crushing force (P_m) and energy absorption (*EA*) of the SW1, DW1, SWFF1 and DWFF1 columns with same impact velocity and impacting mass. The experimental results for SW and DW are 1.54% and 7.80% lower than those of simulations results, respectively, meanwhile, the mean crushing force of the SWFF1 and DWFF1 columns obtained from the experimental are 3.08% and 5.07% higher than those of simulations results, respectively.

The instantaneous crushing force response curves show good agreements between experiments and simulations for overall shape of the curves. The mean crushing force – crushing length curves agree very well for each columns, which show that the finite element models are able to predict the crushing behavior of each column precisely.

From the above observation, it can be concluded that very good agreements can be achieved between experimental and numerical simulation results, and confirmed that the finite element simulations could predict with sufficient accuracy the actual physical behavior and the crushing response of the columns under axial dynamic loading. Hence, for the parametric analysis, the finite element simulations can be performed and a reasonably good result can be expected.

7. Analysis of Foam–Filled Columns

In this section, the crushing behavior of foam–filled columns are analyzed with respect to the mean crushing force response and energy absorption. First, the effect of inserting aluminum foam to the single–walled and double–walled columns is investigated. Then, the effect of core thickness variation was also studied.

7.1. Effect of Aluminum Foam Core

Fig. 18 and Table 7 present crushing force response of SWFF2 and DWFF2 columns compared to those of a SW2 column and DW2 column with the same wall thickness ($t = 1$ mm). In addition, for comparison, also included two more force responses, i.e. SW2+F and DW2+F, which were the sum of force rensponses of column wall and foam when they were loaded separately, as shown in Fig. 19. The first peak force in Fig. 18(a) correspond to the local buckling initiation, and the subsequent peaks represent the progressive plastic deformation modes.

From Fig. 18(b), it is shown that significant increase of mean crushing force and energy absorption can be obtained by inserting aluminum foam to the single–walled and double–walled columns. The increase of crushing force can be easily observed from the mean crushing force – crushing length curve in Fig. 18(b). This is due to the direct compressive strength of the foam and from the interaction between the foam and the wall column. The inserted foam reduces the folding wavelength, hence increases the number of folds formed and thus increases the crushing force response. Similar effects of foam insertion were also found in double–walled foam–filled columns. As can be seen in Table 7, the mean crushing force of SWFF2 is 340% of SW2, the mean crushing force of DWFF2 is 314% of SW2 column, and the mean crushing force of DW2 is 215% of SW2 column. It also can be observed that the foam–filled columns have better performances compared to the sum of force responses of the column walls and foam (SW2+F and DW2+F) when they were loaded separately (See Fig. 19). It is clear that interaction between column wall and the foam will increase the crushing resistance quite significantly.

In Fig. 18(b), the mean crushing force of single–walled foam–filled increases during the development of the folds. This happens because during the folding process, a densification of the

foam occurs, which make further plastic deformation is more difficult to form. On the other hand, the mean crushing force of double–walled foam–filled decreases which indicate that the force response of the walls are more dominant than the foam.

As shown in Fig. 18 and Table 7, the numerical results indicate that after 54.99 mm of the fold distance, the crushing resistance of the single–walled foam–filled column is greater than that of the double–walled foam–filled column because of densification of the foam.

7.2. Effect of Core Thickness Variation

The crushing behavior of DWFF3 column with three different core thickness (C = 7 mm, 8.5 mm, and 10 mm) are analyzed in this section and compared to SWFF3 column. Fig. 20(a) shows the instantaneous crushing force response and Fig. 20(b) shows the mean crushing force response of the columns. The values of the mean crushing force and the energy absorbed by the column are presented in Table 8.

The results show that the mean crushing force of SWFF3 is 107.6% of DWFF3.1, 101.9% of DWFF3.2, and 94.8% of the mean crushing force of DWFF3.3, which clearly shows that the mean crushing force of the double–walled foam–filled column increases as the foam core becomes thicker, as there is more foam material that can absorb impact energy and better interaction between the walls and the foam core. At this stage the optimum core thickness was still not being studied.

8. Normalized Mean Crushing Force and Structural Efficiency

The Specific Energy Absorption (*SEA*) and Crush Force Efficiency (*CFE*) are known as the important crashworthiness parameter to measure the efficiency of the energy aborbing elements, which are defined as

14

$$SEA = \frac{EA}{m_{deformed}} \qquad \text{and} \qquad CFE = \frac{P_m}{P_{max}} \qquad (2)$$

The *SEA* is defined as the ratio of the total energy absorbed (*EA*) by a structure to its deformed mass ($m_{deformed}$). Meanwhile, the *CFE* is defined as the ratio of the mean crushing force to the peak force.

The *SEA* and *CFE* for the SW, DW, SWFF and DWFF columns analyzed in this section are given in Table 7–8.

Fig. 21 and Fig. 22 present P_m, *SEA*, *CFE* for DW, SWFF and DWFF columns normalized by the SW column (P_{m-SW}, SEA_{SW}, CFE_{SW}). Hence, the capability and efficiency of various columns with different geometry in absorbing energy can be directly compared.

In the study of Set 2 and Set 3, SWFF2 have the highest *CFE* compared with other column configurations. Meanwhile, double–walled foam–filled DWFF2 and DWFF3.3 have the highest *SEA* for Set 2 and Set 3, respectively.

9. Conclusions

In this paper, an experimental and numerical study of aluminum foam–filled columns with square cross section under dynamic axial crushing force have been carried out. The results show that inserting the foam to the column will increase the energy absorption capability, which have been shown from the experiments and numerical simulations. The interaction between the foam core and the column wall will change the deformation mode from one localized fold to multiple propagating folds and lead to the increase of total mean crushing force of the column. Similar effects of foam filling were also found in double–walled foam–filled columns. The mean crushing force of single–walled foam–filled column can reach up to 340% of single–walled

column, the mean crushing force of double–walled foam–filled column is 146.2% of double–walled column.

Comparing the analysis results of double–walled foam–filled columns with various core thicknesses of the same outer wall geometry, it is found that increasing the core thickness will increase the crushing force. The results showed that the mean crushing force of double–walled foam–filled column is 105.5% of single–walled foam–filled column.

Acknowledgement

References

[1]   Langseth M. Crashworthiness of light–weight automotive structures 2001 – 2006. In : NorLight conference; 2003.

[2]   Reid J. Crashworthiness of automotive steel mid–rails: thickness and material sensitivity. Thin–Walled Structures, Vol. 26(2), pp. 83–103, 1996.

[3]   Marsolek J, and Reimerdes HG. Energy absorption of metallic cylindrical shells with induced non–axisymmetric folding patterns. International Journal of Impact Engineering, Vol. 30, 1209–23, 2004.

[4]   Simon JW, Kirkpatrick SW. High–speed passenger train crashworthiness and occupant survivability. International Journal Crashworthiness, Vol. 4(2), pp. 121–32, 1999.

[5]   Hayashi. Impact resistant structure for the helicopter and energy absorber used for the same. US Patent, US006959894B2, Nov 2005.

[6]   Kindervater C. Aircraft and helicopter crashworthiness: design and simulation. In: Ambrosio JAC, Pereira MFOS, Silva FP, editors. Proceeding of crashworthiness of transportation systems: structural impact and occupant protection; July 7–19, 1996. Troja/Portugal.

[7]   Thornton P. Energy absorption by foam–filled structures. SAE paper 800081, 1980.

[8]   Santosa SP, Wierzbicki T. Crash behavior of box columns filled with aluminum honeycomb or foam. Computers and Structures, Vol. 68, pp. 343–367, 1998.

[9]   Santosa SP and Wierzbicki T. On the modelling of crush behavior of a closed–cell aluminum foam structure. Journal of Mechanics, Physics, and Solids, Vol. 46(4), pp. 645–669, 1998.

[10] Santosa SP, Wierzbicki T, Hanssen AG, Langseth M. Experimental and numerical studies of foam–filled sections. International Journal of Impact Engineering, Vol. 24(5), pp. 509–534, 2000.

[11] Chen W. Experimental and numerical study on bending collapse of aluminum foam–filled hat profiles. International Journal of Solids and Structures, Vol. 38, pp. 7919–7944, 2001.

[12] Kavi H, Toksoy AK, Guden M. Predicting energy absorption in a foam–filled thin–walled aluminum tube based on experimentally determined strengthening coefficient. Materials and Design, Vol. 27(4), pp. 263–269, 2006.

[13] Niknejad A, Liaghat GH, Moslemi NH, Behravesh AH. Theoretical and experimental studies of the instantaneous folding force of the polyurethane foam–filled square honeycombs. Materials and Design, Vol. 32, Issue 1, pp. 69–75, 2011.

[14] Niknejad A, Abedi MM, Liaghat GH, Nejad MZ. Prediction of the mean folding force during the axial compression in foam–filled grooved tubes by theoretical analysis. Materials and Design, Vol.37, pp. 144–151, 2012.

[15] Santosa SP, Wierzbicki T. The concept of double–walled sandwich columns for energy absorption. International Journal of Crashworthiness, Vol. 4(2), pp. 175–198, 1999.

[16] Seitzberger M, Rammerstorfer FG, Gradinger R, Degischer HP, Blaimschein M, Walch C. Experimental studies on the quasi–static axial crushing of steel columns filled with aluminium foam. International Journal of Solids and Structures, Vol. 37, pp. 4125–4147, 2000.

[17] Zhang Y, Sun G, Li G, Luo Z, Li Q. Optimization of foam–filled bitubal structures for crashworthiness criteria. Materials and Design, Vol 38, pp 99–109, 2012.

[18] Gunawan Leonardo, Jusuf Annisa, Dirgantara Tatacipta, Putra Ichsan Setya. Experimental study on axial impact loading of foam filled aluminum columns. Journal of KONES Power Train and Transport, Vol. 20, No. 2, pp. 150–157, 2013.

[19]   Hanssen AG, Hopperstad OS, Langseth M, Ilstad H. Validation of constitutive models applicable to aluminum foams. International Journal of Mechanical Sciences, Vol. 44, pp. 359–406, 2002.

[20]   Jing Bi, Hongbing Fang, Qian Wang, Xuchun Ren. Modeling and optimization of foam–filled thin–walled columns for crashworthiness designs. Finite Elements in Analysis and Design, Vol. 46, pp. 698–709, 2010.

[21]   Avallone EA, Baumeister T, Sadegh A. Marks' standard handbook for mechanical engineering. New York: McGraw Hill; 2006.

[22]   Hallquist JO. LS–DYNA theoretical manual. California: Livermore Software Technology Corporation, 1998.

[23]   Langseth M, Hopperstad OS, Berstad T. Crashworthiness of aluminium extrusions: validation of numerical simulation, effect of mass ratio and impact velocity. International Journal of Impact Engineering, Vol. 22, pp. 829–854, 1999.

[24]   Abramowicz W, Jones N. Dynamic axial crushing of square tubes. International Journal of Impact Engineering, Vol. 2, No. 2, pp. 179–208, 1984.

[25]   Abramowicz W, Jones N. Dynamic progressive buckling of circular and square tubes. International Journal of Impact Engineering, Vol. 4, No. 4, pp. 243–270, 1986.

[26]   Gunawan L, Dirgantara T, Putra I.S. Development of a dropped weight impact testing machine. International Journal of Engineering and Technology IJET–IJENS, Vol. 11(06), pp. 120–126, 2011.
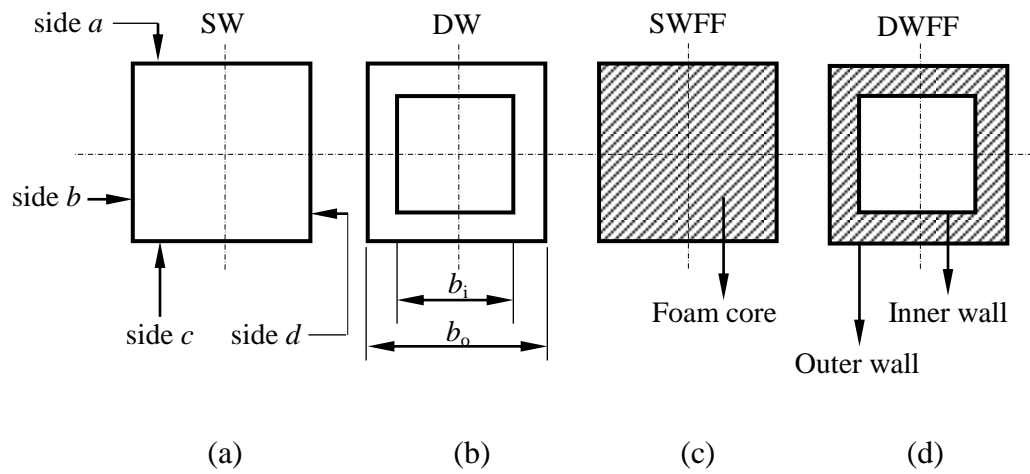
Figure 1. Geometry of the columns (a) single–walled (SW), (b) double–walled (DW), (c) single–walled foam–filled (SWFF), and (d) double–walled foam–filled (DWFF)
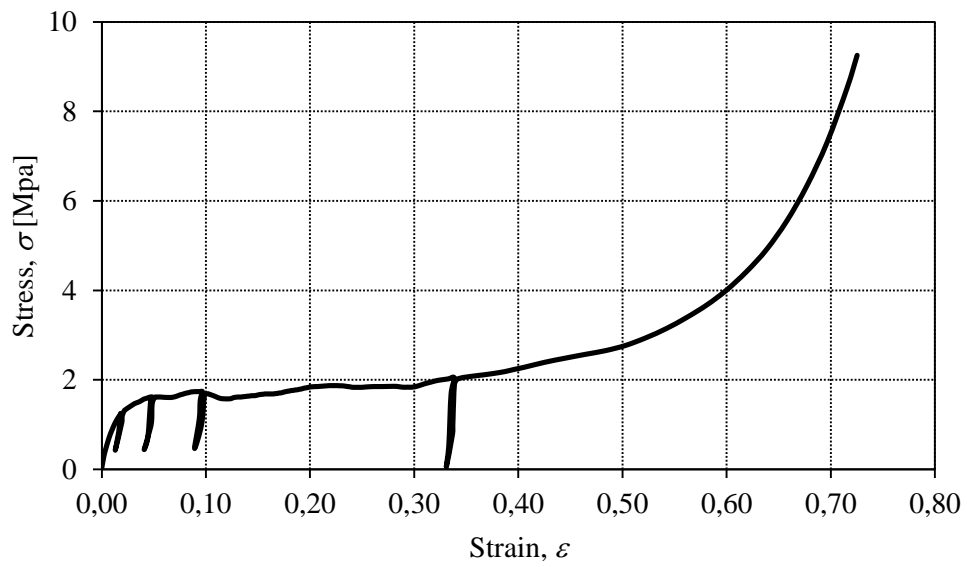
Figure 2. Compressive stress–strain curve of ALPORAS
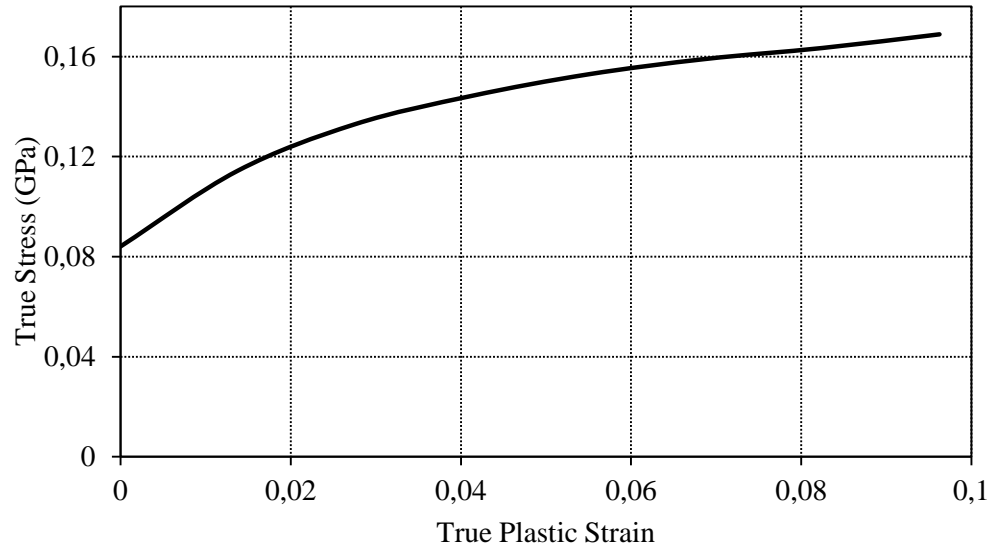
Figure 3. True stress–true plastic strain curve of AA6063–T1

Impacting
Mass

$2H$ — Geometrical
Imperfection location

Direction of
Rigid body
translation

Single–walled foam–filled
column isometric view :

Thin–walled
column

Fixed
constraint
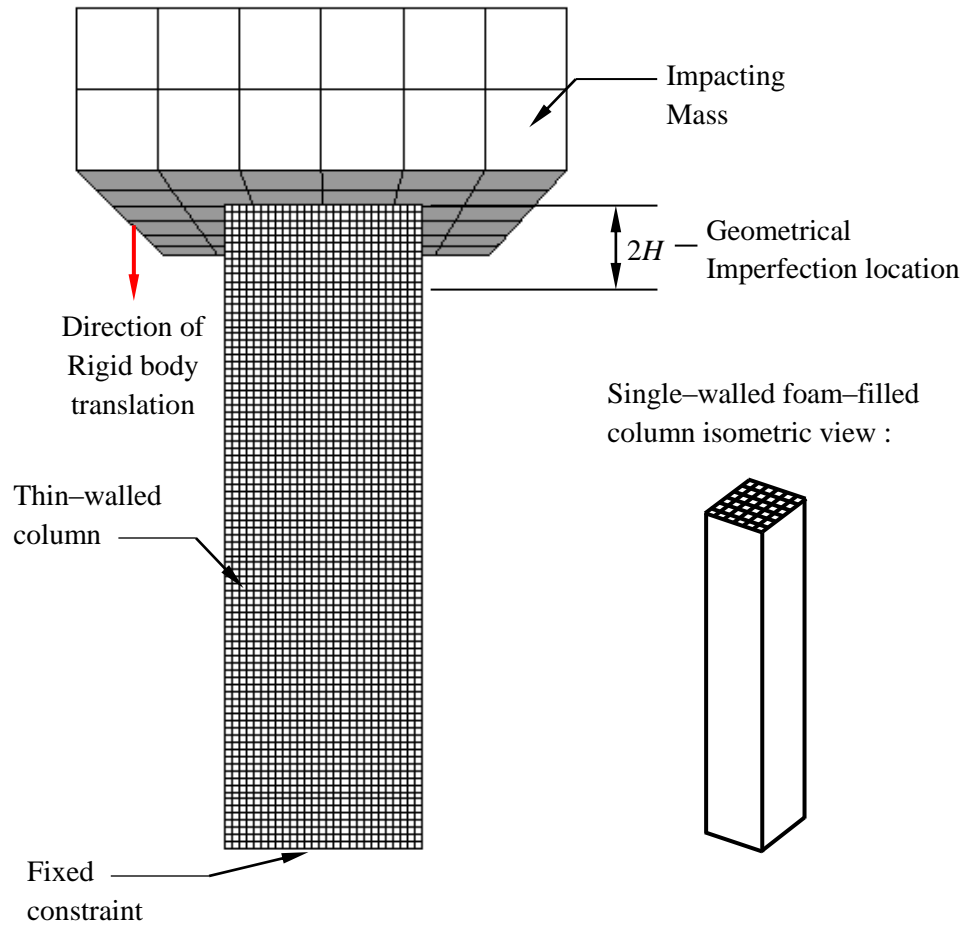
Figure 4. Finite element model of a foam–filled column

(a)

(i)   (ii)   (iii)
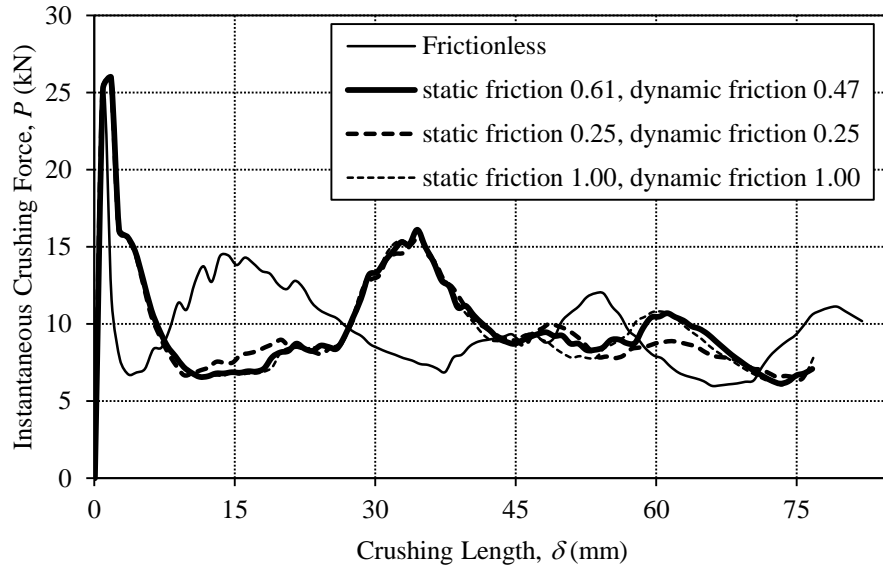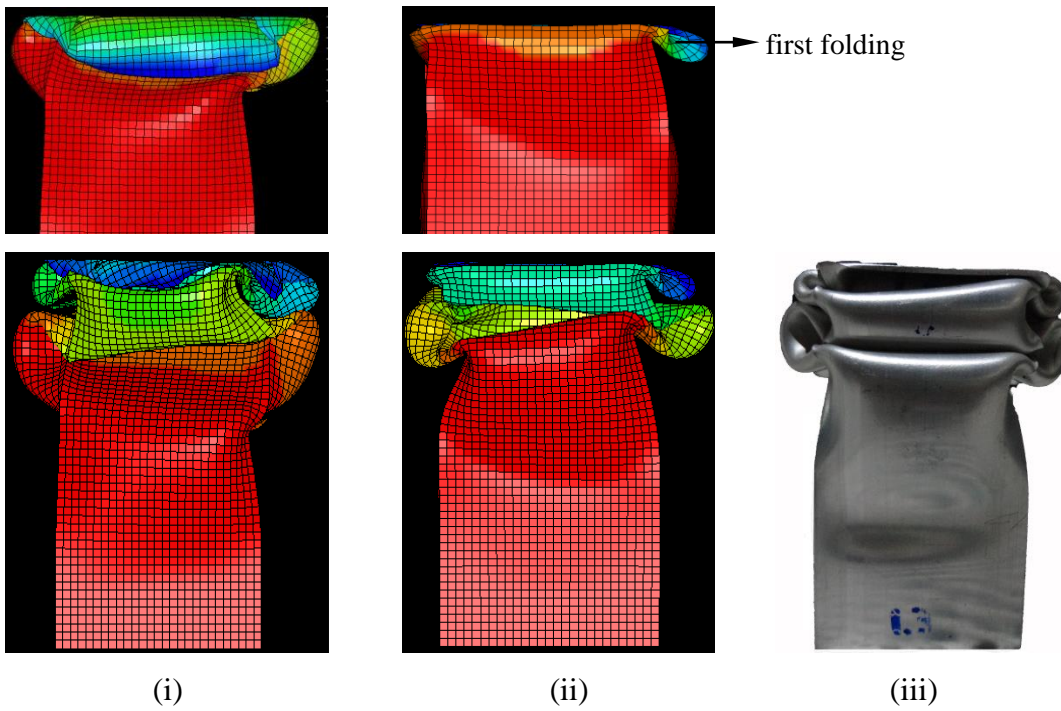
(b)

Figure 5. (a) Crushing response of aluminum alloy square columns with different friction coefficients, and (b) Plastic deformation modes of square columns (i) frictionless, (ii) $\mu_s = 0.61$, $\mu_d = 0.47$, (iii) experimental result
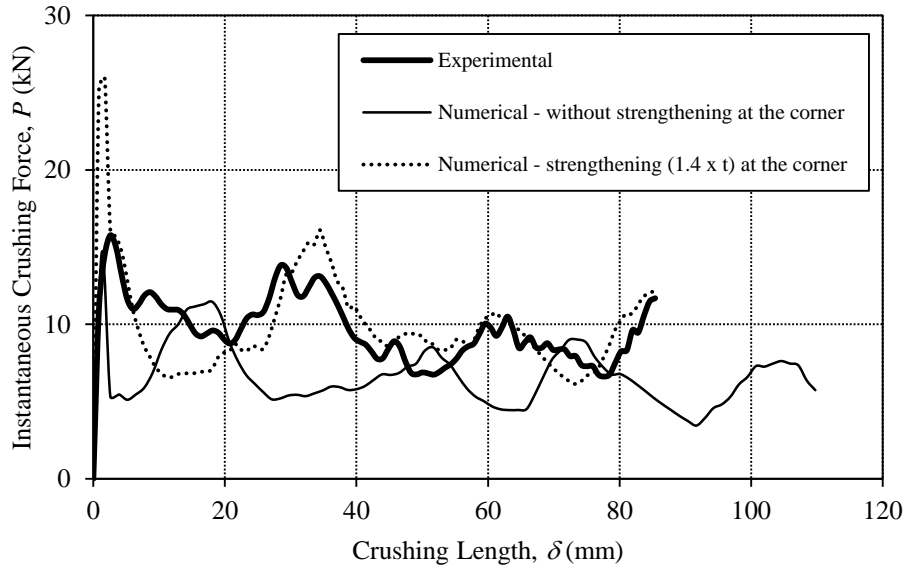
(a)
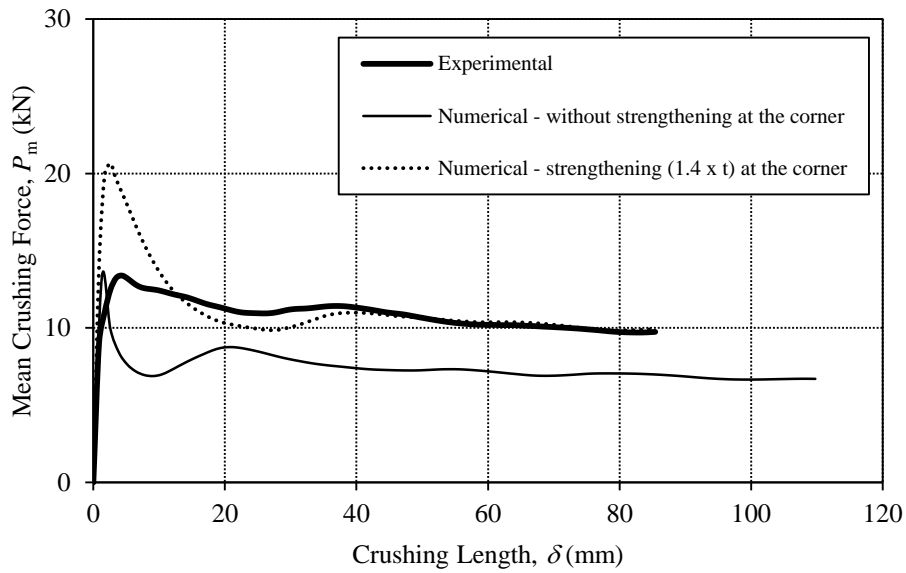
(b)

Figure 6. Crushing response of the extruded aluminum alloy columns experimental result
compared with numerical simulations with the effect of strengthening at the corners

25

(a)   (b)   (c)
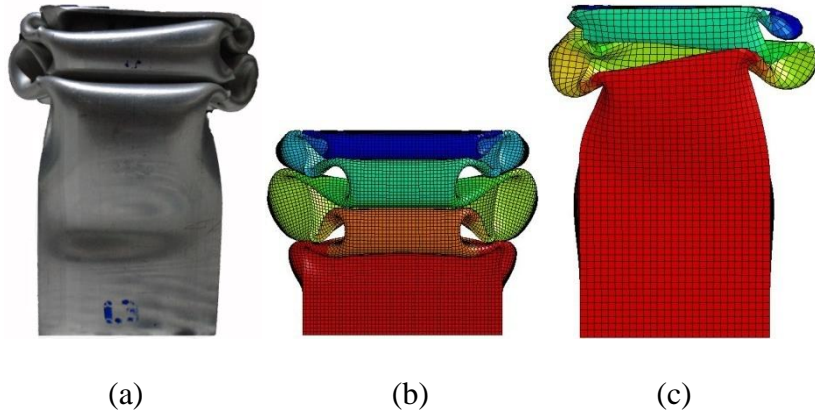
Figure 7. (a) Experimental result, (b) Finite element model of the extruded aluminum column

Set 1 without strengthening, (c) with strengthening at the corners $t_c = 1.4 \times t$

thickness of the column wall $= t$

thickness of the column wall $= t \times \sqrt{2}$
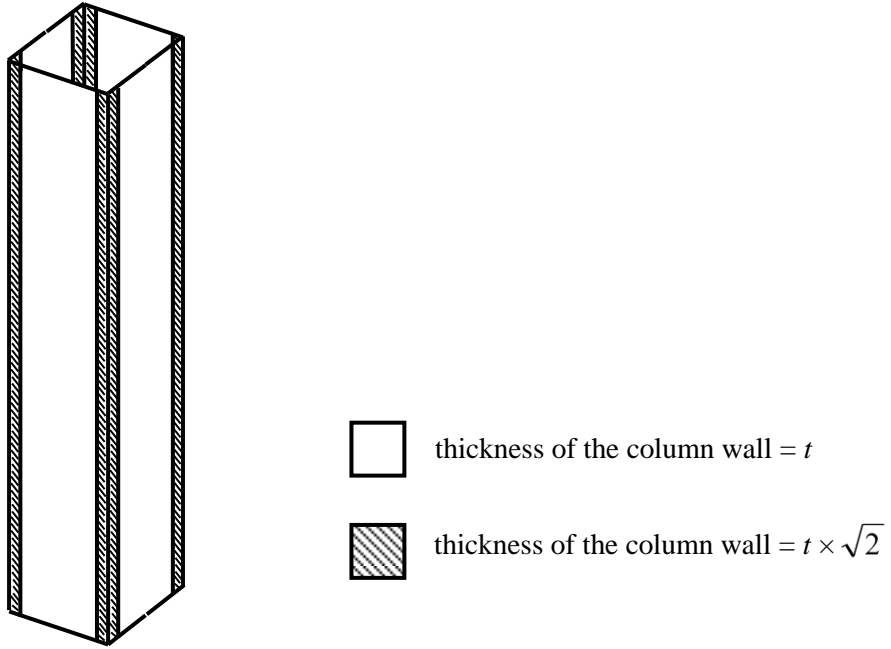
Figure 8. Finite element model of the extruded aluminum alloy column

Set 1 with strengthening at the corners
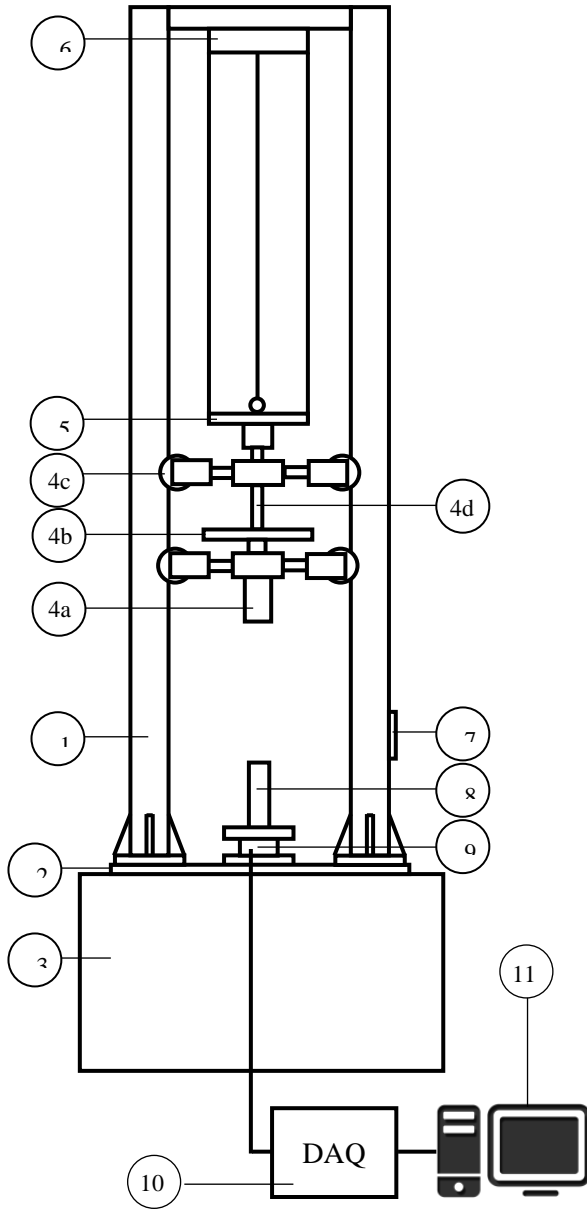
No.	Name	Qty.
1.	Guide columns	2
2.	Steel plate	1
3.	Concrete base	1
4.	Impactor assembly	
	a. Impactor head	1
	b. Weightening mass	
	c. Wheels	4
	d. Frame	1 set
5.	Clamp	1
6.	Hoist	1
7.	Speed sensor	1
8.	Specimen	
9.	Load cell	1
10.	Data Acquisition System	1
11.	Computer	1

(a)   (b)

Figure 9. (a) Schematic drawing and (b) picture of dropped weight impact testing machine [26]
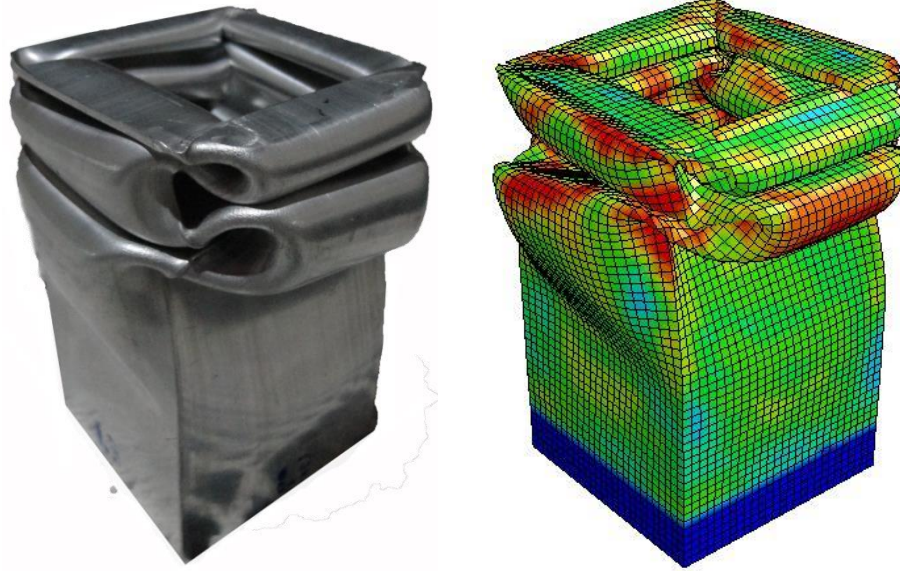
<center>(a)   (b)</center>

Figure 10. Deformation modes of aluminum alloy SW1 column

(a) Experimental result (SW1–E) [18], (b) Numerical result (SW1–N)
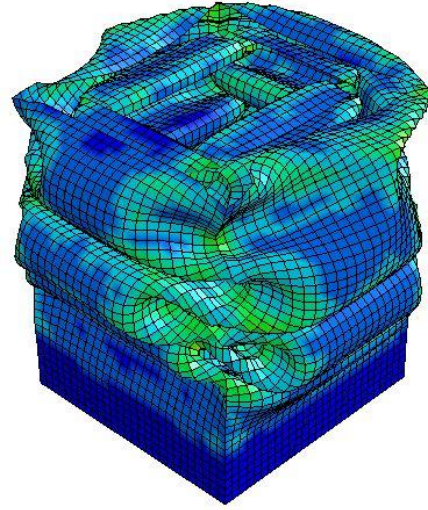
<center>(a)   (b)</center>

Figure 11. Deformation modes of aluminum alloy DW1 column

(a) Experimental result (DW1–E) [18], (b) Numerical result (DW1–N)

(a)   (b)
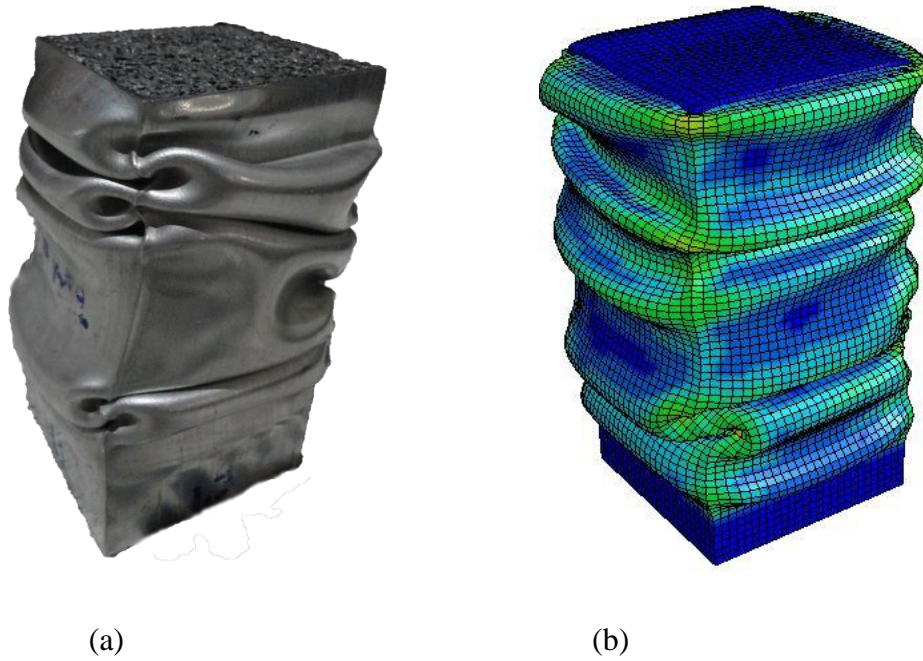
Figure 12. Deformation modes of single–walled foam–filled (SWFF1) column
(a) Experimental result (SWFF1–E) [18], (b) Numerical result (SWFF1–N)

<div align="center">(a)   (b)</div>
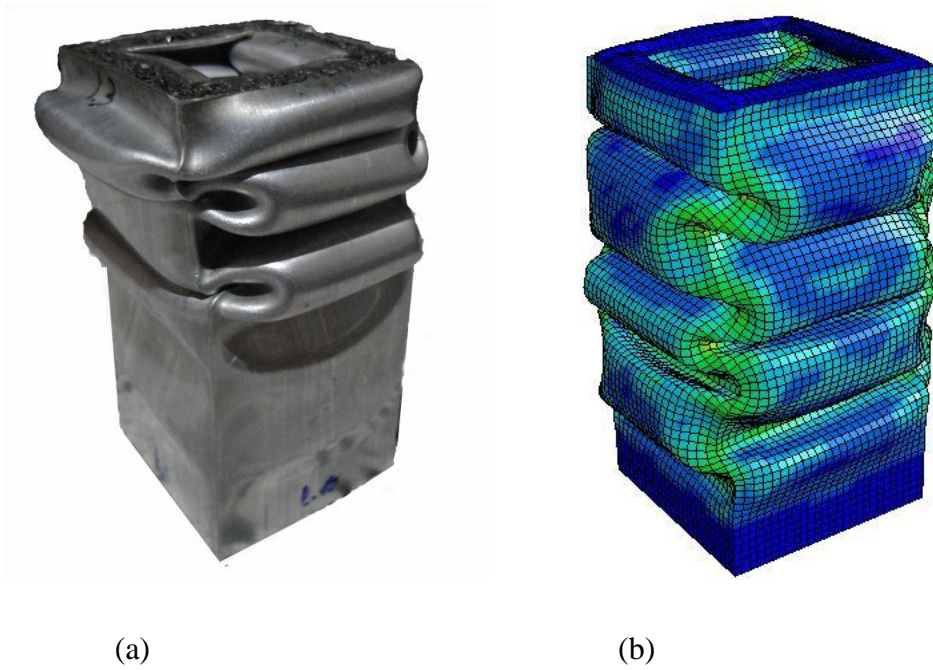
Figure 13. Deformation modes of double–walled foam–filled (DWFF1) column
(a) Experimental result (DWFF1–E) [18], (b) Numerical result (DWFF1–N)
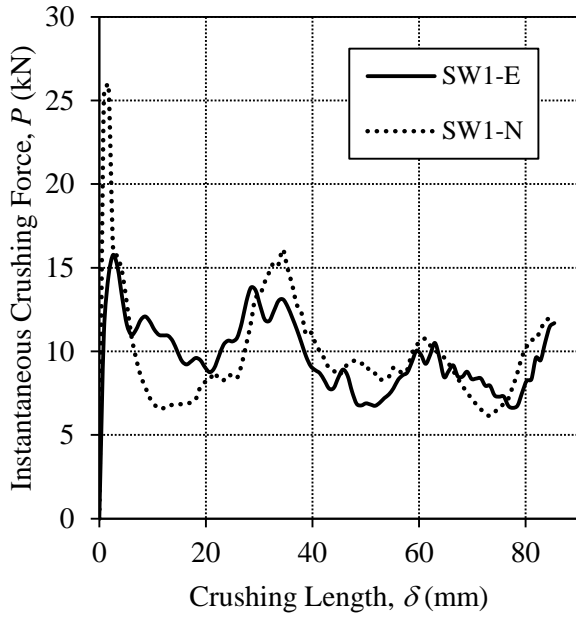
Figure 14. Crushing responses of single–walled (Set 1–SW1) columns

(a) Experimental result (SW1–E) [18], (b) Numerical result (SW1–N)
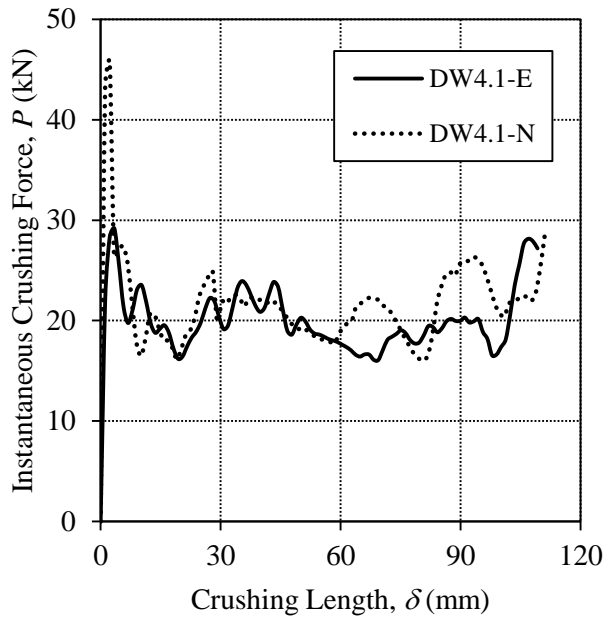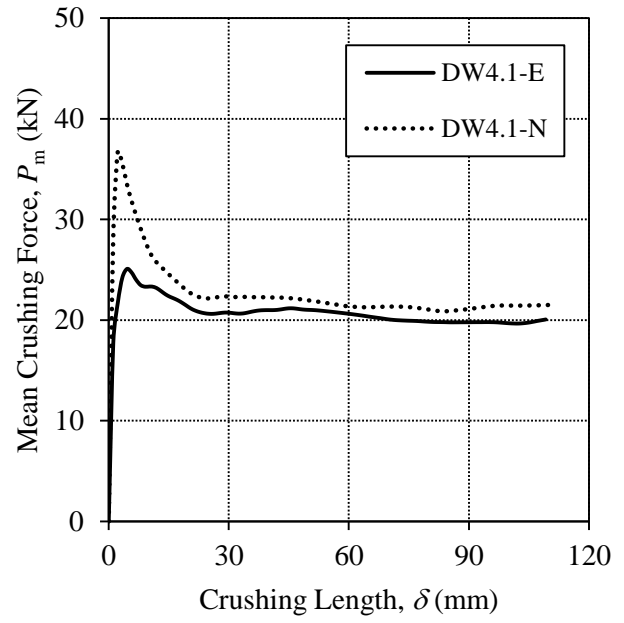
Figure 15. Crushing responses of double–walled aluminum alloy (Set 1 – DW1) columns

(a) Experimental result (DW1–E) [18], (b) Numerical result (DW1–N)
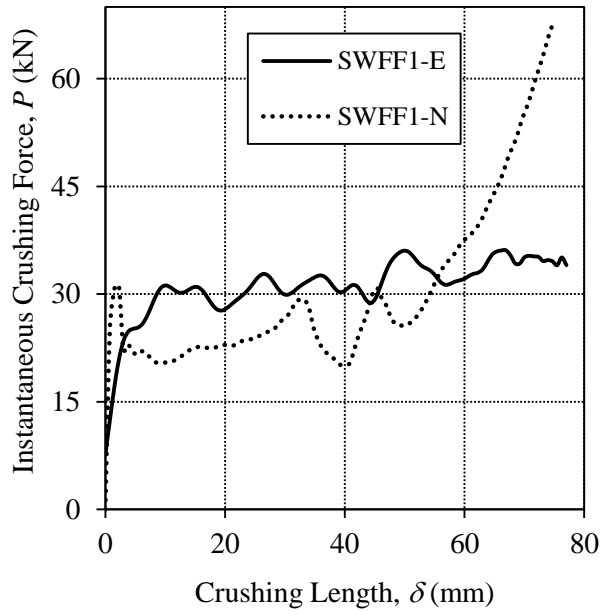
Figure 16. Crushing responses of single–walled foam–filled (Set 1–SWFF1) columns

(a) Experimental result (SWFF1–E) [18], (b) Numerical result (SWFF1–N)
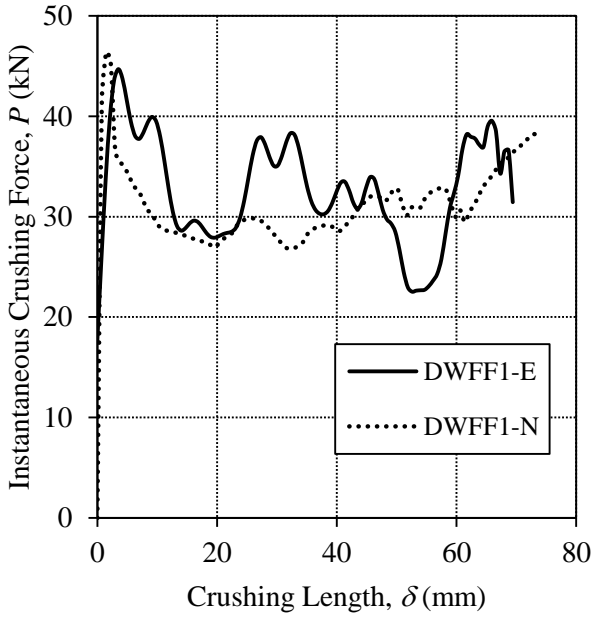
Figure 17. Crushing responses of double–walled foam–filled (Set 1–DWFF1) columns

(a) Experimental result (DWFF1–E) [18], (b) Numerical result (DWFF1–N)
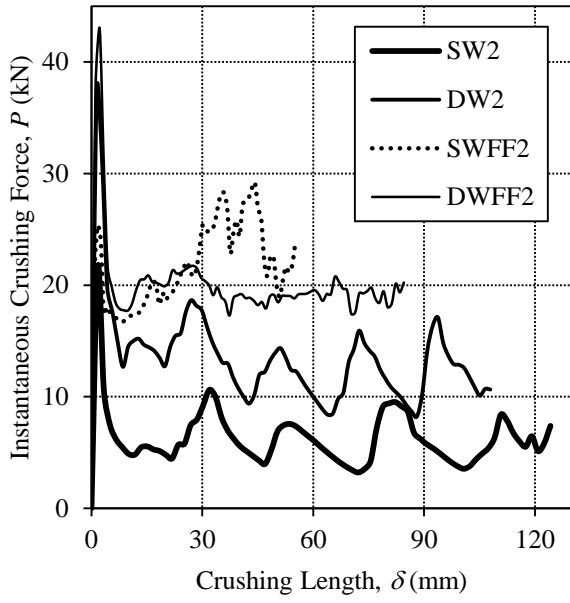
(a)
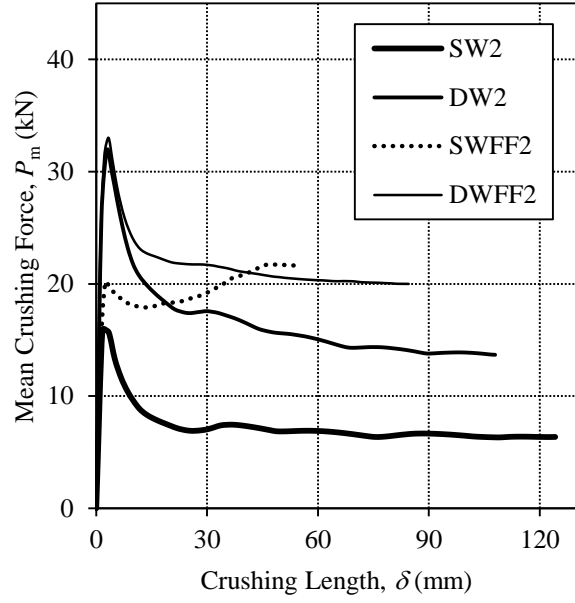
(b)

Figure 18. Crushing responses of Set 2 – SW2, DW2, SWFF2 and DWFF2 columns

with the effect of aluminum foam core
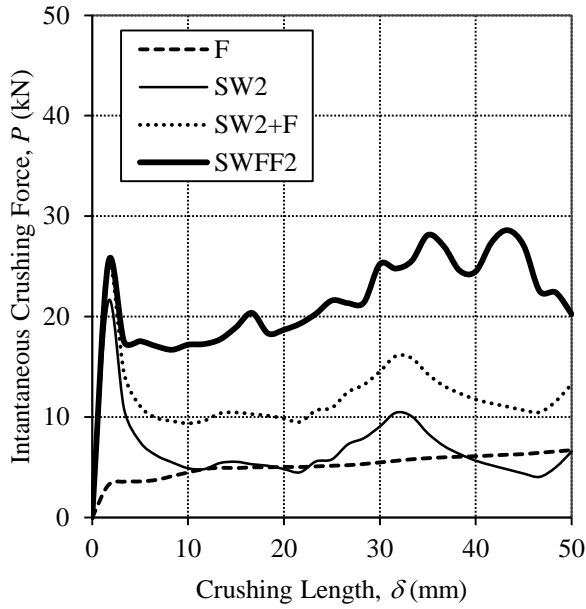
(a)
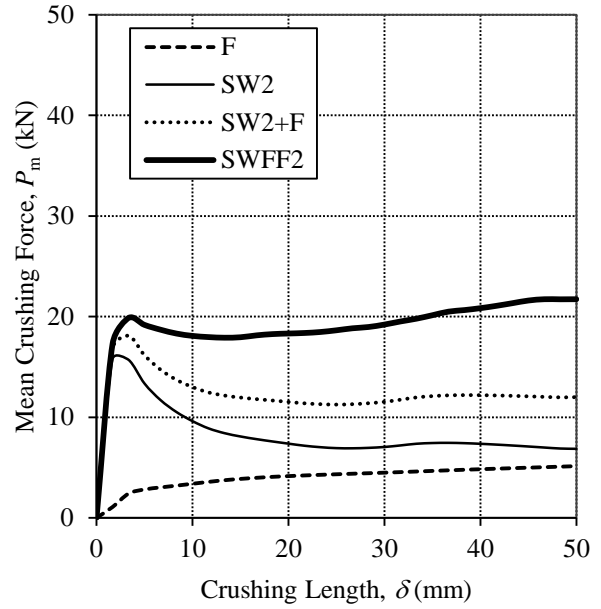
(b)
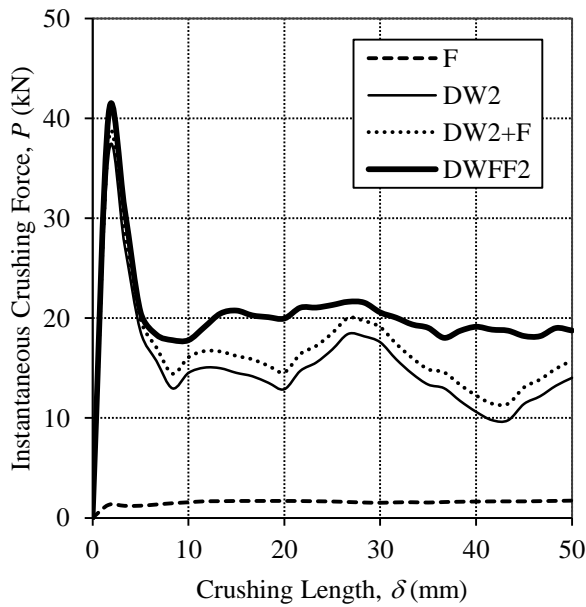
(c)
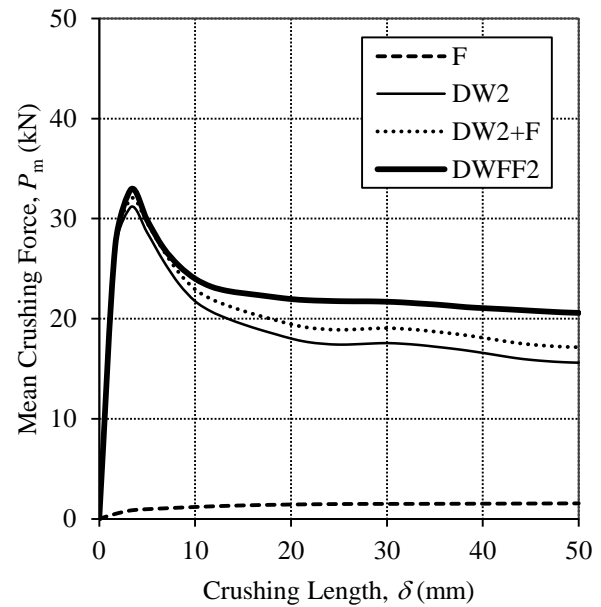
(d)

Figure 19. Crushing responses of Set 2 – (a)(b) SW2, F, SW2+FF2 and SWFF2

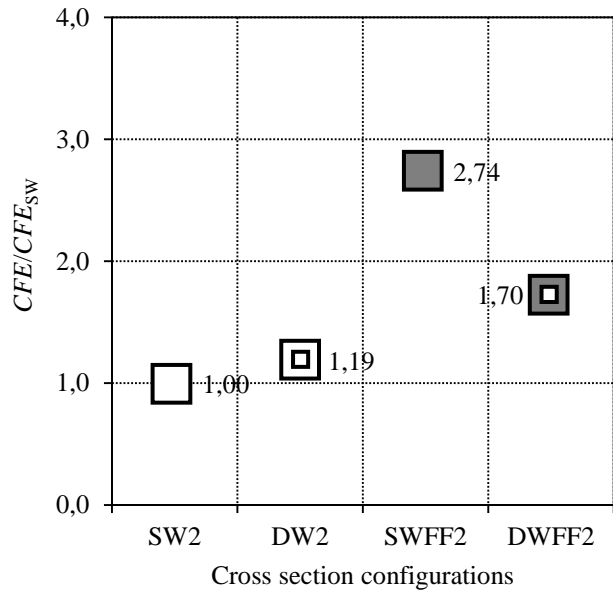(c)(d) DW2, F, DW2+F and DWFF2 columns

38
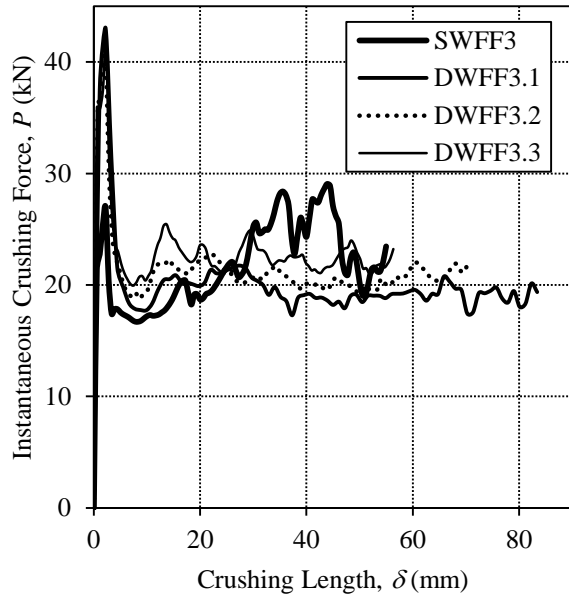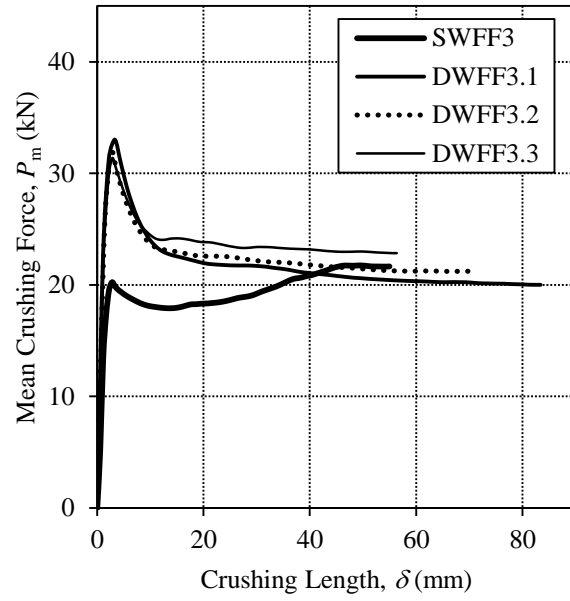
(a)   (b)

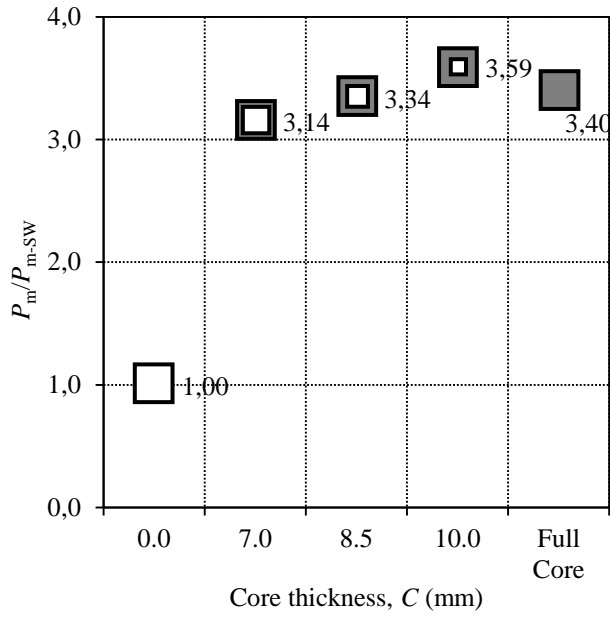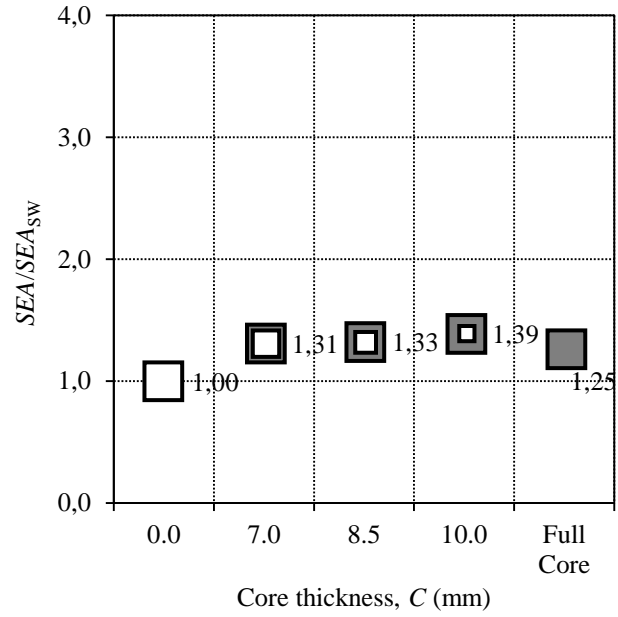Figure 20. Crushing responses of Set 3 – SWFF3 and DWFF3 columns with the effect of core
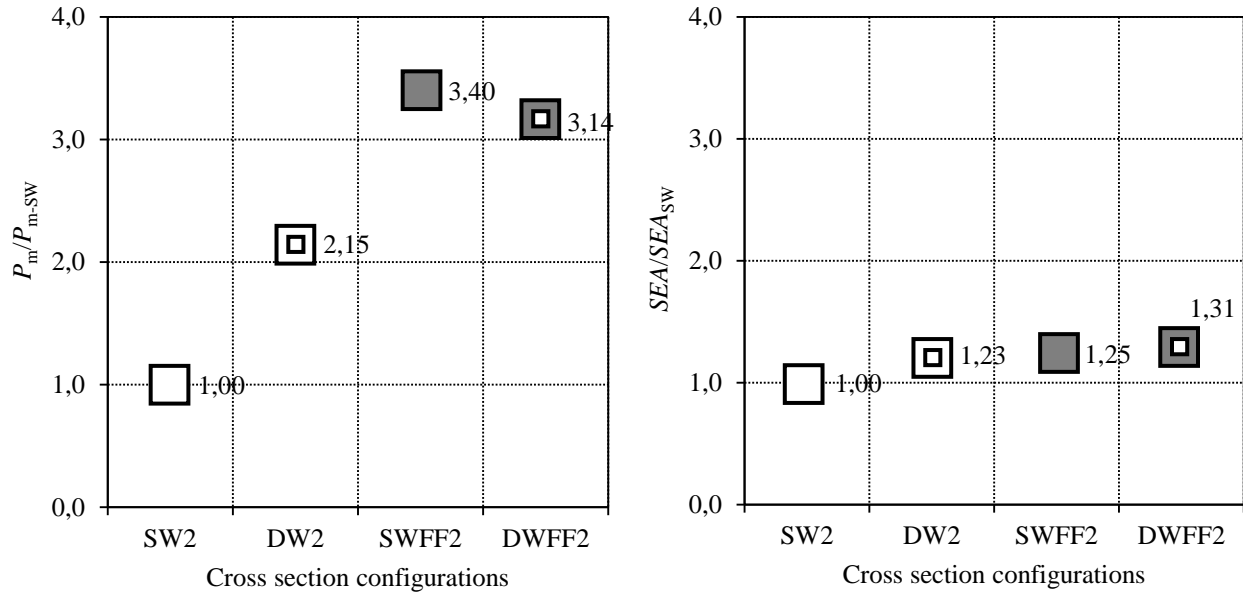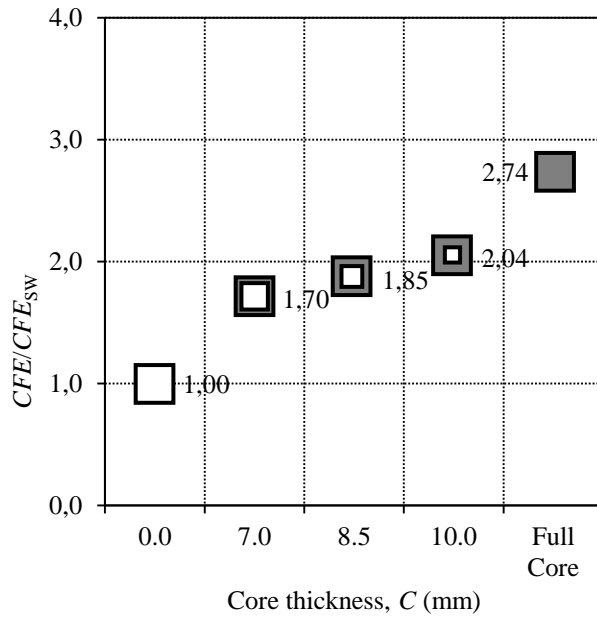
thickness

Figure 21. (a) $P_m/P_{m–SW}$, (b) SEA/SEA_{SW}, and (b) CFE/CFE_{SW} for the foam–filled columns with

constant thickness ($t = 1.10$ mm) and constant $b_i/b_o = 0.75$

(a)

(b)

(c)

Figure 22. (a) P_m/P_{m-SW}, (b) SEA/SEA_{SW}, and (b) CFE/CFE_{SW} for the foam–filled columns with

constant column thickness ($t = 1.10$ mm)

Table 1. Geometrical detail of the foam–filled columns for Set 1

(Numerical and Experimental Analysis)

		SW & SWFF		DW & DWFF			
		Outer Column Thickness t_o (mm)	Outer Column Width b_o (mm)	Outer Column Thickness t_o (mm)	Outer Column Width b_o (mm)	Inner Column Thickness t_i (mm)	Inner Column Width b_i (mm)
side	a	1.30		1.30		1.10	
	b	1.30	55.00	1.30	55.00	1.10	38.00
	c	1.10		1.10		1.10	
	d	1.00		1.00		1.10	

42

Table 2. Geometrical detail and impact parameters of the columns for Set 1, 2, 3, 4
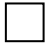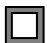
	Code	Column Thickness t (mm)	Outer Column Width b_o (mm)	Inner Column Width b_i (mm)	Column Mass m_c (kg)	Impact Velocity v (m/s)	Impact Mass m_i (kg)
		Set 1 (Numerical and Experimental Analysis)					
□	SW1				0.125	6.10	45.5
▣	DW1		(as in Table 1)		0.222	7.95	75.63
■	SWFF1				0.342	7.73	75.63
▣	DWFF1				0.311	7.80	75.63
		Set 2 (Numerical Analysis, Effect of Aluminum foam core)					
□	SW2			–	0.118		
▣	DW2	1.10	55	41	0.211	8.00	80
■	SWFF2			–	0.340		
▣	DWFF2			41	0.281		
		Set 3 (Numerical Analysis, Effect of core thickness)					
■	SWFF3			–	0.340		
▣	DWFF3.1	1.10	55	41	0.281	8.00	80
▣	DWFF3.2			38	0.295		
▣	DWFF3.3			35	0.306		

Table 3. Material properties of ALPORAS and AA 6063–T1

	ALPORAS	AA6063–T1
Young's modulus, E (MPa)	540	$7.32 \ 10^4$
Yield stress, σ_y (MPa)	1.702	83.81
Poisson's ratio, ν	0.30	0.30

Table 4. P_m and δ of aluminum columns with different friction coefficients

Static and Dynamic Friction Coefficient	P_m (kN)	δ (mm)
Frictionless	9.59	88.18
$\mu_s = 0.61$, $\mu_d = 0.47$ [21 – 22]	9.92	85.26
$\mu_s = 0.25$, $\mu_d = 0.25$ [23]	9.85	85.96
$\mu_s = 1.00$, $\mu_d = 1.00$	9.89	85.55

Table 5. P_m and δ of aluminum columns with the effect of corner strengthening

	P_m (kN)	δ (mm)
Experimental	9.76	85.46
Numerical – without strengthening at the corner	6.62	127.84
Numerical – strengthening (1.4×t) at the corner	9.93	85.27

Table 6. Set 1 – numerical and experimental results of the columns

	P_{max} (kN)	δ_{max} (mm)	E_A (kJ)	P_m (kN)	P_m difference (%)
SW1–E [18]	16.00	85.46	0.83	9.76	
SW1–N	26.14	88.04	0.85	9.61	1.54
DW1–E [18]	29.53	112.75	2.25	19.99	
DW1–N	45.93	110.99	2.39	21.55	7.80
SWFF1–E [18]	36.13	77.02	2.30	31.10	
SWFF1–N	67.96	74.93	2.26	30.14	3.08
DWFF1–E [18]	44.69	69.54	2.27	32.72	
DWFF1–N	46.89	74.12	2.30	31.06	5.07

*Experimental result (E), Numerical result (N)

Table 7. Set 2 – numerical analysis results of aluminum alloy SW2, DW2, SWFF2 and DWFF2

columns with the effect of aluminum foam core

Code	m (kg)	P_{max} (kN)	δ_{max} (mm)	P_m (kN)	EA_{total} (kJ)	SEA_{total} (kJ/kg)	EA_{δ} (kJ)	SEA_{δ} (kJ/kg)	CFE
							$\delta = 54.99$ mm		
F	0.208	6.61	54.99	6.61	0.53	5.69	0.29	4.46	1.00
SW2	0.118	23.17	124.17	6.36	0.79	9.75	0.38	10.55	0.27
DW2	0.205	42.24	107.92	13.68	1.48	12.03	0.85	13.28	0.32
SW2 + F	0.326	24.67	54.99	11.97	0.67	6.57	0.67	6.57	0.48
DW2 + F	0.281	37.65	54.99	17.15	0.93	10,57	0.93	10,57	0.45
SWFF2	0.326	29.19	54.99	21.65	1.19	12.14	1.19	12.14	0.74
DWFF2	0.281	43.86	83.93	20.00	1.68	12.82	1.12	12.73	0.46

Table 8. Set 3 – numerical analysis results of aluminum alloy SWFF3 and DWFF3 columns

with the effect of core thickness

Code	t (mm)	m (kg)	$P_{\max}$ (kN)	$\delta_{\max}$ (mm)	P_{m} (kN)	EA_{total} (kJ)	SEA_{total} (kJ/kg)	EA_{δ} (kJ)	SEA_{δ} (kJ/kg)	CFE
								$\delta = 54.99$ mm		
SWFF3		0.326	29.19	54.99	21.65	1.19	12.14	1.19	12.14	0.74
DWFF3.1		0.281	43.86	83.93	20.00	1.68	12.82	1.12	12.72	0.46
DWFF3.2	1.10	0.295	42.59	70.39	21.22	1.49	12.96	1.17	12.72	0.50
DWFF3.3		0.306	41.68	56.30	22.84	1.29	13.58	1.26	13.26	0.55